Broadening and shift of CH_4 triplet 6046.96 cm^{-1} and its components induced by collisions with SF_6 molecules

V.A. Kapitanov, Yu.N. Ponomarev, I.S. Tyryshkin, A.D. Bykov, and V.N. Savel'ev

Institute of Atmospheric Optics, Siberian Branch of the Russian Academy of Sciences, Tomsk

Received February 12, 2008

The results of measurements and calculations of broadening and shift coefficients for unresolved triplet 6046.96 cm^{-1} of CH_4 and its components due to collisions with SF_6 molecules are presented. The measurements were realized by using a high-sensitive photo-acoustic spectrometer with a diode laser providing for a spectral resolution of $7 \cdot 10^{-4}$ cm^{-1} and a signal-to-noise ratio more than 10^3. The obtained results are in satisfactory agreement with the experimental data.

Introduction

The peculiarity of absorption spectra of highly symmetric molecules, such as CH_4, is the presence of multiplets, i.e., groups of lines with strong overlapping. As is known, the cluster structure of a spectrum arises from tetrahedral separation of rotational-vibrational energy levels confluent to null approximation. The separation is narrow at small quantum numbers of angular momentum, but enhances at their growing. The multiplet components totally overlap at sufficiently high buffer gas pressure. As a result, a problem of their separation and determination of their parameters arises when analyzing methane spectra. One more reason of interest to the study of CH_4 multiplets is that the effects of spectral exchange are easily observable for them, which lead to distortion of the profile shape and redefinition of its parameters. Investigation of broadening and shift of CH_4 absorption lines and shapes of multiplet profiles allows a detailed study of different manifestations of spectral line interference in molecular gases; this is important when developing spectroscopic methods of laser gas analysis with tunable narrow-band lasers.

Half-widths of methane absorption lines at pressure variations of nitrogen, oxygen, air, and rare gases were measured and calculated repeatedly.[1–16] At present, there is a large body of numerical data required for different applications. Half-widths of methane absorption lines were calculated with the Anderson–Tsao–Carnatte (ATC)[3,4] method on the assumption of the CH_4 octopole moment linearity, the magnitude of which was chosen to reproduce experimental data. High coupling terms were taken into account in calculations, up to hexadecapole-hexadecapole, as well as induction and dispersion forces.

Calculations[1,5,6] were carried out on the base of more rigorous Robert–Bonamy method with accounting for the short-range part of potential, represented as a sum of pair atom-atomic potentials. Accurate rovibrational wave functions, accounting for trajectory bending, were also used in calculations. A satisfactorily general agreement between calculated and measured coefficients of broadening and shift of lines of ν_3 band induced by nitrogen pressure was obtained; however, some other factors, caused by the symmetry type of transition-connected states, should be taken into account for accurate reproduction of experimental data.

The profile of multiplet methane lines has been analyzed with accounting for interference between its components.[7–16] Nitrogen and rare gases were considered as buffer ones. Multiplets with small J are not resolved in basic bands, therefore, calculations were carried out for multiplets with $J > 5$, for which tetrahedral separation is sufficiently large and individual components are observed under Doppler broadening. The formation of cluster profiles at $J \sim 20$ was considered in Ref. 11. The influence of temperature and buffer gas parameters on calculations of absorption coefficients was studied in Refs. 13–16. Formation of profiles for the "forbidden" ν_2 band was studied in Ref. 12; line broadening of the ν_1 band in the Raman spectrum was investigated in Ref. 14.

The principal conclusion of these works is that spectral exchange becomes apparent already at low pressures of a buffer gas, which leads to a significant deviation of absorption coefficients from the sum of Voigt profiles of individual lines.

The problem of our interest was the broadening and shift of lines, induced by collisions of CH_4 molecule with SF_6 ones, which are also highly symmetric. As is known, the methane molecule in equilibrium configuration has a symmetry of T_d group, its equilibrium values of dipole and quadrupole moments are zero, and the octopole moment is the first nonzero one. The SF_6 molecule has the point symmetry group O_h, and the first nonzero moment is hexadecapole. Therefore, the main electrostatic interaction in CH_4 and SF_6 collisions is octopole-hexadecapole, proportional to the intermolecular distance R^{-8}. The second in value is interaction between hexadecapole moments of CH_4 and SF_6, proportional to R^{-9}. The main part of polarization potential (disperse interaction)

0235-6880/08/07 493-07 $02.00

is a summand proportionate to R^{-6}. Thus, broadening of lines induced by collisions of highly symmetric CH_4 and SF_6 molecules is determined by short-range interacting forces.

Note also that rovibrational interaction in highlynsymmetric molecules results in nonzero mean values of dipole and quadrupole moments. The dipole moment for the ground state of CH_4 molecule has been calculated[17,18] and measured,[19] its magnitude is not high ($(5.38 \pm 0.10) \cdot 10^{-6}$ D). The induced dipole moment for excited vibrational states is significantly higher. The calculated and measured values of mean dipole moment for the (0010) vibrational state of CH_4 molecule are given in Refs. 20 and 21, where the induced dipole moment turns out to be 0.02 D, which is as much as four times higher than for the ground vibrational state.

The vibration-induced mean dipole moment depends on the number of excited vibrational quanta of ν_3 or ν_4. Therefore, it is expected for overtone bands that additions, caused by intramolecular interactions will result in a noticeable change in intermolecular potential, e.g., due to appearance of the dipole-dipole interaction depending on intermolecular distance R^{-3} in case of self-broadening. Thus, long-range dipole interactions can definitely contribute to broadening coefficients of methane lines, connected with transitions to excited vibrational states.

This circumstance was not taken into account in previous calculations of line broadening and shift coefficients in the CH_4–SF_6 mixture, because the majority of related works was devoted to line broadening and shift in basic vibrational bands.

This work presents the calculation and measurement results on broadening and shift coefficients of 6046.96 cm^{-1} triplet line of methane molecule induced by SF_6 broadening. The measurements have been carried out using a high-sensitive acoustic spectrometer allowing a signal-to-noise ratio of about 10^3. Owing to high resolution and sensitivity, the study of individual triplet components is possible. The broadening and shift coefficients of individual components have been calculated as well; the calculation results are in satisfactory agreement with the measured ones.

The broadening coefficients for the CH_4–SF_6 pair were measured earlier[22] for the P7F line of ν_3 band; the calculated data for this line are given in Ref. 23, they are in a good agreement with the experiment, the difference is 10%. Measurements and calculations for the methane lines in mixture with SF_6 were not carried out earlier for the triplet under study.

1. Experiment

The two-channel PA spectrometer with a diode laser (DOAS DL) was used for the measurements. Its block-diagram is shown in Fig. 1; the main spectrometer specifications are given in Table 1.

Table 1. OAS specifications

Parameter	Value
Spectral range, cm^{-1}	6040–6300
Spectral resolution, cm^{-1}	0.0007
Signal-to-noise ratio	1000

A TEC-100 semiconductor laser with an external cell (Sacher Laser Technik) generates continuous single-frequency radiation within 6040–6300 cm^{-1} range with a radiation spectrum width of ~10 MHz and an output power of 0.003–0.01 W. The radiation power is controlled with a photodetector, built into the laser unit, and modulated with a variable frequency optical chopper Model 300C (SCITEC INSTRUMENTS).[24]

The lasing frequency is controlled with a diffraction grating. Manual rotation of the grating with a microscrew allows the laser tuning to any wavelength of the given range, while the rotation with a piezoelectric ceramic element executes continuous

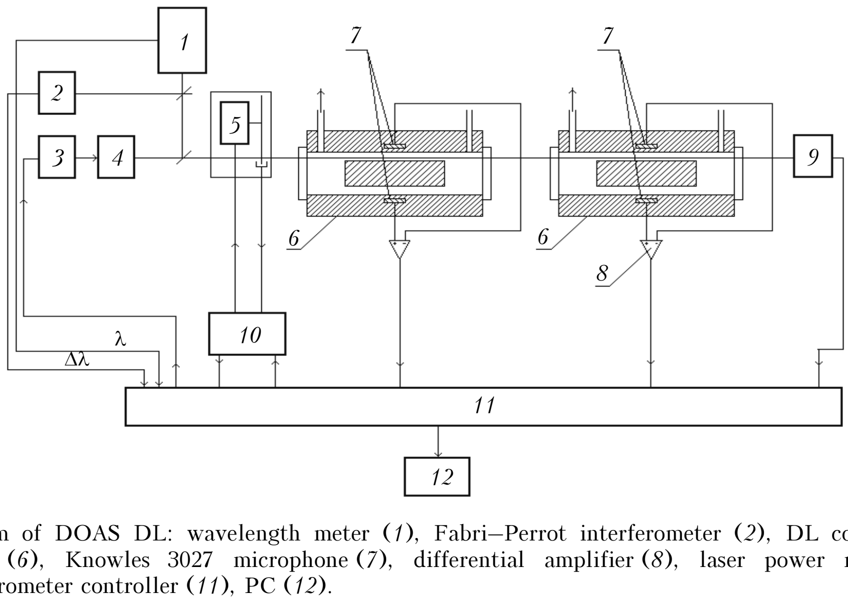

Fig. 1. Block-diagram of DOAS DL: wavelength meter (*1*), Fabri–Perrot interferometer (*2*), DL controller (*3*), DL (*4*), modulator (*5*), PAD (*6*), Knowles 3027 microphone (*7*), differential amplifier (*8*), laser power meter (*9*), modulator controller (*10*), spectrometer controller (*11*), PC (*12*).

(without mode jumps) controller-controllable radiation retuning within a range 0.001–3 cm^{-1}. An electric signal, controlling the piezoelectric ceramic element, is produced by a twelve-digit digital-to-analog converter (DAC); it changes the voltage from 0 to 100 V according to a specified program with a minimal step of about 0.024 V, which corresponds to about 22-MHz (0.00073 cm^{-1}) step of the frequency tuning.

Measurement and manual adjustment of lasing wavelength to a preset initial wavelength are carried out with the help of a wavelength meter (WS-7 117 IR-type WLM, "Angstrom Ltd."[25]). An error of absolute measurements of the initial wavelength ($\Delta\nu/\nu$) does not exceed 10^{-6}.

Lasing frequency in the program-controllable tuning is controlled with a Fabry–Perot etalon of IT-28–30 type with 3 and 10 cm bases (0.1666 and 0.05 cm^{-1} free spectral ranges). To exclude the influence of air pressure drops on the free spectral range, the Fabry–Perot etalon is placed into a hermetically sealed casing filled with dry nitrogen under atmospheric pressure.

A PAD with a cell in the form of differential Helmholtz resonator (DHR) was used as a high sensitive resonance PA detector with a low level of acoustic noises.[26]

The Helmholtz resonator has a great advantage: acoustic vibrations in HR cells at a resonance frequency are antiphased. Since microphones are located in each cell, the difference of acoustic signals can be recorded (the so-called differential Helmholtz resonator). In this case, the useful signal is doubled and in-phase external acoustic noise decreases by 1–2 orders of magnitude. The used design of DHR with two capillaries is totally symmetric and allows a low level of external noise even in a gas flow. When the gas flow passes through both DHR cells, in-phase acoustic noise is formed in each of them and is subtracted by the differential amplifier.

The measurements were carried out within a range 6046.8–6047.15 cm^{-1} and at SF_6 pressure from 0 to 500 Torr at a room temperature.

The measurement technique and spectrometer design are described in more detail in Ref. 27.

2. Determination of line parameters

The line under study is a triplet, including (0 3 F2 1) → (4 4 F1 142), (0 3 F1 1) → (4 4 F2 142), and (0 3 A2 1) → (4 4 A1 1) transitions centered at 6046.9420, 6046.9527, and 6046.9647 cm^{-1}, respectively. "Exact" quantum numbers are given in parenthesis: the number of resonance polyad, angular moment J, symmetry type, and the number of a given level in ascending order.

The profile parameters of individual triplet components were determined by the least-squares method in two ways. In the first way, the profile of each multiplet component was considered as a Voigt one; in the second, a profile, accounting for line interference,[7] was used:

$$\alpha(x,y) = \frac{1}{\gamma_D \pi^{3/2}} \int_{-\infty}^{\infty} \frac{\xi y + \eta(x-t)}{(x-t)^2 + y^2} e^{-t^2}\, dt,$$

where parameters x and y have usual meanings:

$$x = (\omega - \omega_0)/\gamma_D, \quad y = \gamma/\gamma_D$$

and $\gamma_D = \omega_0\sqrt{2kT/mc}$ is the Doppler half-width of a line. The second item under the integral is caused by the spectral exchange between multiplet components and depends on the cross-correlation factor η.

Line centers and half-widths, ξ and η for spectra, recorded at different buffer gas pressures, were determined by fitting. Figure 2 shows the measured and calculated profiles of a 6046.96 cm^{-1} line and their difference. Note that the difference between measured and calculated absorption coefficient does not exceed 0.5%. The line interference changes the profile parameters; in this case, ξ, being an analogue of line strength, depends on the buffer gas pressure.[7]

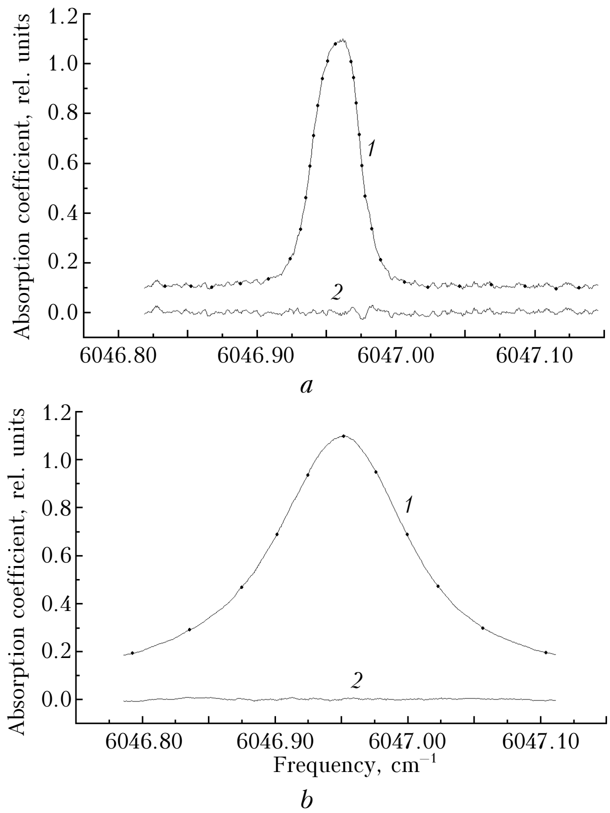

Fig. 2. Total profile of methane absorption lines centered at 6046.9420, 6046.9527, and 6046.9647 cm^{-1}, respectively. SF_6 pressure is 39.5 (*a*) and 493.5 Torr (*b*). Curve *1* corresponds to experimental data and curve *2* to the difference between experimental and calculated values normalized to the maximum calculated value. The methane pressure equals to 4.5 Torr in both spectra.

Therefore, we determined ξ separately for each value of SF_6 pressure. Finally, the coefficients of linear dependence of this parameter on the broadening gas pressure were obtained (Figs. 3–5).

The fitting results are given in Table 2 along with the calculated half-widths and shifts.

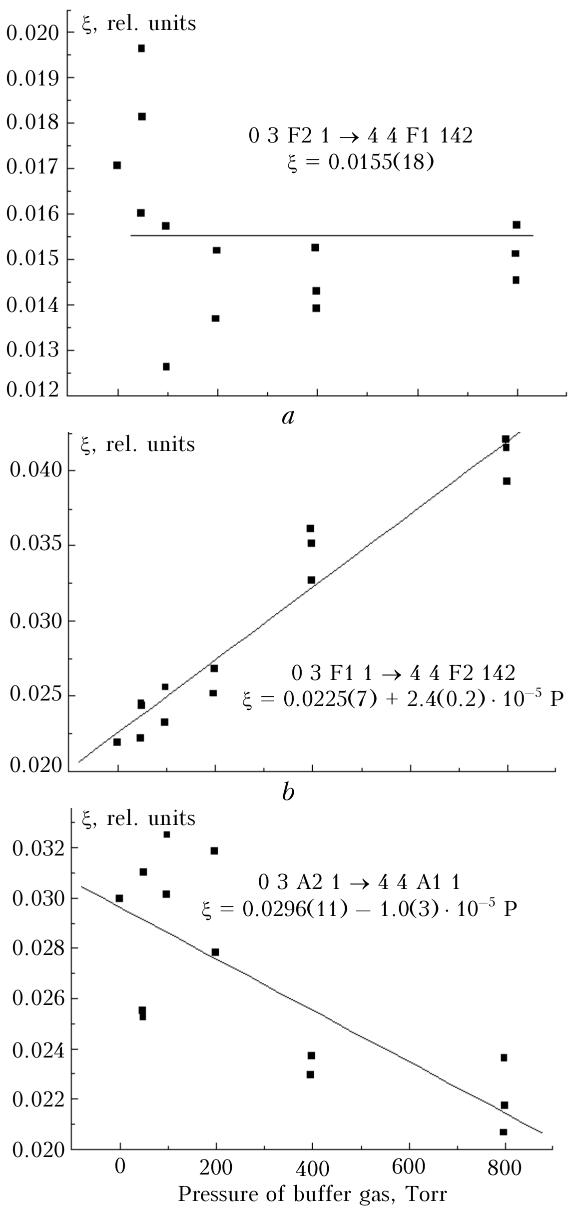

Fig. 3. The parameter ξ of the CH_4 triplet component 6046.9420 cm^{-1} (*a*), 6046.9527 cm^{-1} (*b*), and 6046.9647 cm^{-1} (*c*) as a function of SF_6 pressure.

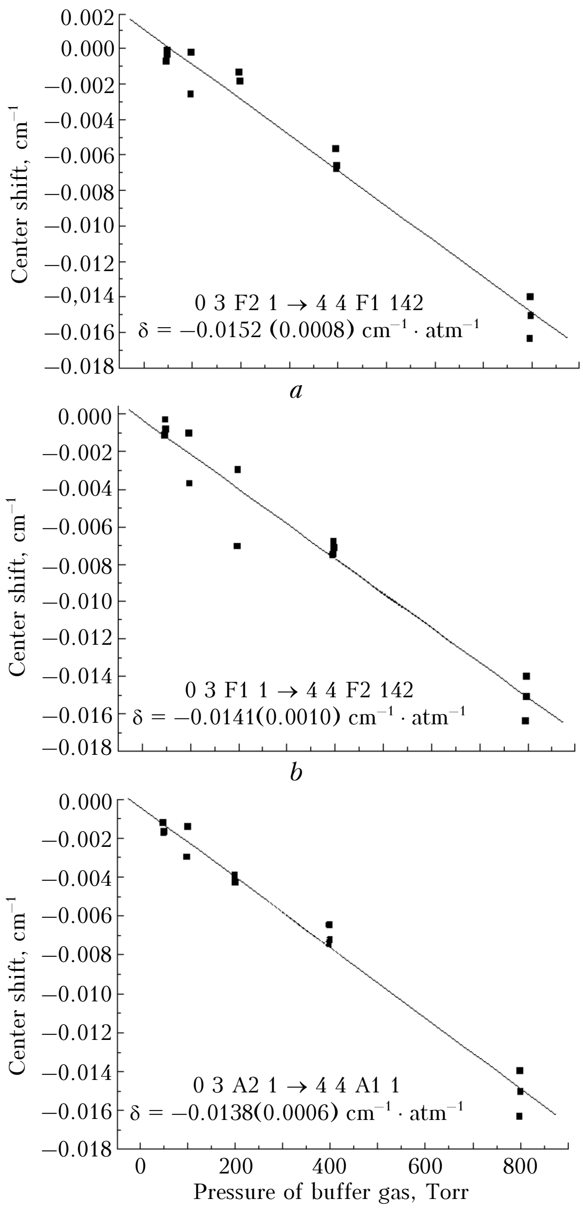

Fig. 4. Shift of the CH_4 triplet component 6046.9420 cm^{-1} (*a*), 6046.9527 cm^{-1} (*b*), and 6046.9647 cm^{-1} (*c*) as a function of SF_6 pressure.

Table 2. Measured and calculated half-widths and shifts of components of CH_4 triplet 6046.96 cm^{-1} induced by SF_6 pressure broadening (in 10^{-3} cm^{-1}/atm)

Parameter	0 3 F2 1 → 4 4 F1 142* 6046.9420	0 3 F1 1 → 4 4 F2 142* 6046.9527	0 3 A2 1 → 4 4 A1 1* 6046.9647
Half-width, exp.	74.1 ± 4.4	95.1 ± 2.9	65.4 ± 2.2
Half-width, calc.	68	68	68
Shift, exp.	–15.4 ± 0.8	–13.7 ± 0.9	–13.6 ± 0.8
Shift, calc.	–36	–36	–36
		Mean values	
Half-width, exp.		78.2	
Half-width, calc.		68	
Shift, exp.		–14	
Shift, calc.		–36	

N o t e . *Quantum numbers of states *P J C n*, where *P* is the polyad number, *J* is the quantum number of angular momentum, *C* is the symmetry type, *n* is the number of level of this symmetry in the ascending order.

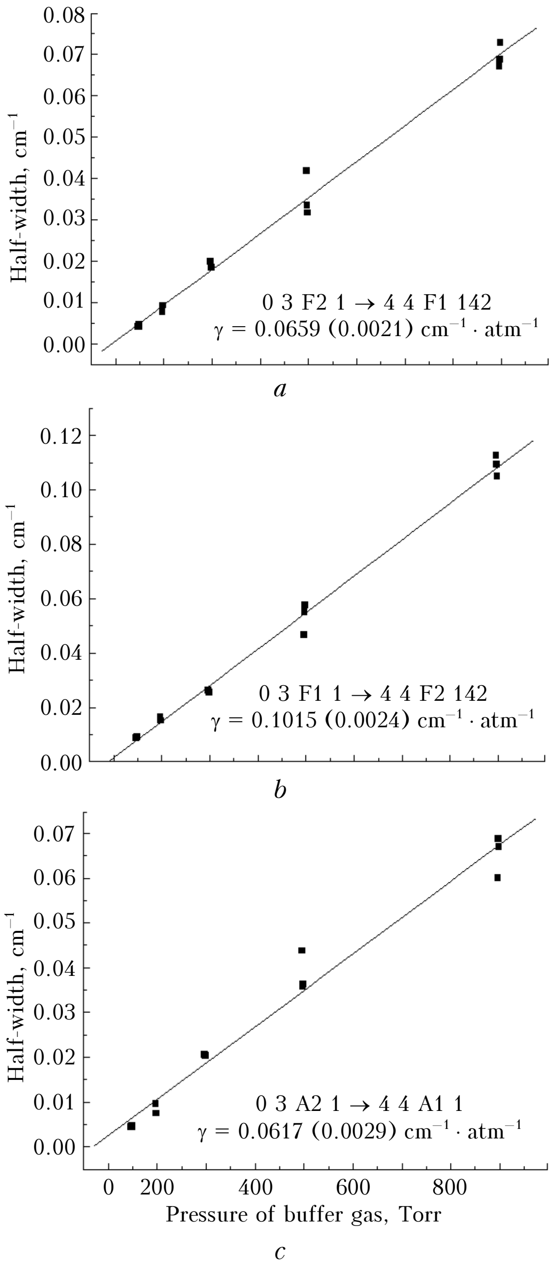

Fig. 5. Half-width of the CH_4 triplet component 6046.9420 (*a*), 6046.9527 (*b*), and 6046.9647 cm^{-1} (*c*) as a function of SF_6 pressure.

Error assessments given in Table 2 are 68%-confidence intervals. Note, that half-widths and shifts for all three lines linearly depend on the SF_6 pressure, and the confidence intervals do not exceed 10% of the determined parameters. Thus, the conclusion can be drawn that measurements of the total triplet profile with a high signal-to-noise ratio allow reconstruction of half-width and shift of individual components using an ordinary technique for experimental data processing.

The following conclusion can be drawn from the analysis of the total line profile: redistribution of intensities of individual components takes place as the buffer gas pressure increases. Note that such effect is to be observed at line interference, since the parameter, determined from the fitting, is in fact a certain combination of "true" intensities.

3. Calculations of broadening and shift coefficients

In the semiclassical impact broadening theory, the half-width γ_{if} and center shift δ_{if} of the line, corresponding to the $i \to f$ transition, are defined as

$$\gamma_{fi} + i\delta_{fi} = \frac{n}{c}\sum_p \rho(p)\int_0^\infty \mathrm{d}v v f(v)\int_0^\infty \mathrm{d}b b U(i,f,p,b,v), \quad (1)$$

where n is the density of thermostat particles; c is the light velocity; $\rho(p)$ is the population of the pth level of a broadening particle; v is the relative velocity; $f(v)$ is the Maxwell distribution function; b is the impact parameter. Summation over the states of exciting molecule and integration over relative velocity and impact parameter are the averaging over all collisions. The complex function $U(i,f,p,b,v)$ determines a contribution of one collision with the impact parameter b and initial velocity v into line broadening and shift; it is expressed via the real and imaginary parts of the truncation function of the Anderson theory:

$$\mathrm{Re}U(i,f,p,b,v) = 1 - \cos\left[\mathrm{Im}S(b)\right]\exp\left[-\mathrm{Re}S(b)\right]; \quad (2)$$

$$\mathrm{Im}U(i,f,p,b,v) = \sin\left[\mathrm{Im}S(b)\right]\exp\left[-\mathrm{Re}S(b)\right]. \quad (3)$$

The truncation function $S(b)$ is represented as a series in terms of powers of intermolecular interaction operator

$$S(b) = S_1(b) + S_2(b) + \ldots . \quad (4)$$

These equations allow the effectiveness function to be calculated even at close collisions, when the perturbation theory is not applicable.

To a certain approximation, the isotropic part of the intermolecular potential is represented as a sum of induction and dispersion potentials. In this case, $S_1(b)$ can be written as

$$S_1(b) = i\frac{3\pi}{8\hbar v b^5}\alpha_2\left\{\langle v_i|\mu^2|v_i\rangle - \langle v_f|\mu^2|v_f\rangle + \right.$$
$$\left. + \frac{3\varepsilon\varepsilon_2}{2(\varepsilon+\varepsilon_2)}\left[\langle v_i|\alpha|v_i\rangle - \langle v_f|\alpha|v_f\rangle\right]\right\}. \quad (5)$$

Here μ is the dipole moment of an absorbing molecule; ε and ε_2 are the ionization potentials of absorbing and broadening particles, respectively; α and α_2 are their polarizabilities. Equation (5) takes into account only the main item of the isotropic part of induction and dispersion interactions.

The vibrational dependence of the isotropic part of intermolecular potential, manifesting itself in the adiabatic shift of levels (5), allows explanation of the strong effect of vibrational excitation in line shift coefficients. Note that an increase in adiabatic item of the truncation function with an enhancement of vibrational excitation is to be taken into account in calculations of line half-widths as well, as at strong excitations they can increase by 10–30%. The difference between mean polarizability values in Eq. (5) can be also determined from the fitting to experimental data on pressure-induced line shifts of the appropriate buffer gas (e.g., rare gases); the obtained data can be used in calculations of coefficients of broadening and shift by pressure of any gases.

Analyzing the second-order summand in Eq. (4), consider the case of collisions between CH_4 and SF_6 molecules. As it is mentioned above, the first nonzero multipole moment is octopole for methane and hexadecapole for SF_6. Hence, the principal electrostatic interaction is octopole-hexadecapole. Besides, higher hexadecapole-hexadecapole, induction, and dispersion interactions should be also taken into account when calculating line broadening and shift coefficients.

As it is mentioned above, a permanent dipole moment of CH_4 is absent due to high symmetry of the molecule, and rotational transitions are forbidden within one vibrational state. However, this interdict is not strict, and, as a consequence, weak, so-called “forbidden,” dipole transitions are intensified due to intramolecular interactions, Coriolis interaction, anharmonicity of vibrations, and centrifugal distortion. The performed analysis has shown the accounting for a weak dipole moment in F_2-symmetry vibrational states, induced by anharmonic interactions, to be necessary. Thus, the interaction potential is represented as

$$V(\mathbf{R}) = V_{d\theta}(\mathbf{R}) + V_{o\theta}(\mathbf{R}) + V_{\theta\theta}(\mathbf{R}) + V_{\text{disp}}(\mathbf{R}) + V_{\text{ind}}(\mathbf{R}). \qquad (6)$$

Here the combinations of subscripts d, o, θ mean dipole, octopole, and hexadecapole interactions, respectively. Expressions for individual items in the second-order truncation function $S_2(b)$ are known.[3] As an example, write the equation for contribution of octopole-hexadecapole potential to the truncation function:

$$S_2^{\Omega\Theta}(b) = \frac{1024}{875}\left(\frac{\Omega_1\Theta_2}{\hbar v}\right)^2 \frac{1}{b^{10}} \times \left\{ \begin{array}{l} \left(1+\delta_{0K_i}\right)^{-1} \sum\limits_{j_2' j_i' K_i'} \left(1+\delta_{0K_i'}\right)^{-1} \times \\ \times\left[C_{j_iK_i32}^{j_i' K_i' \ 2} + C_{j_iK_i3-2}^{j_i' K_i' \ 2} + C_{j_iK_i3-2}^{j_i' -K_i' \ 2} \right] \times \\ \times C_{j_iK_i20}^{j_i' K_i' \ 2} \times \left[f_4(k) + If_4(k) \right] + (i \to f)^* \end{array} \right\}, \qquad (7)$$

where $(i \to f)$ means the addition of the similar summand with replacing i by f; Ω_1 and Θ_2 are the octopole and hexadecapole moments of CH_4 and SF_6, respectively; C_{abcd}^{ef} are the Clebsch–Gordan coefficients; $f_4(k)$ and $If_4(k)$ are the real and imaginary parts of resonance functions. The adiabatic parameter

$$k_{ii'pp'} = \frac{2\pi cb}{v}\left[E_i - E_{i'} + E_p - E_{p'}\right] \qquad (8)$$

depends on the difference between rovibrational energy levels.

Parameters, required for calculations, are given in Table 3. Polarizability of CH_4 in the ground and (0020) vibrational states has been determined from the data of Ref. 28, the CH_4 octopole and SF_6 hexadecapole moments – from Ref. 22, other data – from Ref. 29; the dipole moment for methane in the ground state has been taken from Ref. 19 and for (0020) excited state – from Ref. 20.

Table 3. Molecular parameters of CH_4 and SF_6

Parameter	CH_4	SF_6
Rotational constant, cm^{-1}	5.24059	0.09111
Centrifugal constant, cm^{-1}	$1.086 \cdot 10^{-4}$	$1.6 \cdot 10^{-8}$
Dipole moment, D	$\mu_{0000} = 5.38 \cdot 10^{-6}$ $\mu_{0020} = 4.0 \cdot 10^{-2}$	0
Quadrupole moment, D · Å	0	0
Octopole moment, D · Å^2	2.6	0
Hexadecapole moment, D · Å^3	4.8	30.0
Polarizability, Å^3	$\alpha_{0000} = 2.264$, $\alpha_{0020} = 2.662$	4.475
Ionization potential, eV	12.98	15.7

The calculations were carried out at a room temperature in approximation of linear molecule and mean velocity according to Eqs. (2)–(8). All levels up to $J_p = 100$ were taken into account when averaging over the broadening particle states. The calculation results are given in Table 2.

Conclusion

The performed measurements have shown that a 6046.95 cm^{-1} line profile becomes noticeably asymmetric (see Fig. 2) as the buffer gas pressure increases due to the presence of three lines with different intensities. Mutual fitting of their parameters allowed determining the half-width and shift coefficient, as well as cross-relaxation coefficients of all three triplet components (see Figs. 3–5). Two ways of fitting give similar results; accounting for pressure dependence of ξ is seemingly equivalent to accounting for the spectral exchange and cross-relaxation parameters η.

Emphasize that the difference in centers of three triplet components is not large and does not exceed 0.025 cm^{-1} (0.0022 cm^{-1} at the Doppler half-width). Measurements with accounting for the pressure dependence of absorption coefficients and with a high signal-to-noise ratio allow totally overlapping individual parameters of lines to be determined with confidential intervals not higher than 10%.

The calculated line half-widths satisfactorily agree with the mean measured parameters. The differences for individual lines are 5, 8, and 40%, while the difference is 14% for the mean half-width. Note also that fitting parameters were not used in calculations of shift coefficients.

As is known, equation (5) describes the dispersion interaction only approximately; in fact, the dependence of dispersion energy on integrals containing electron wave function is more complicated. Note that the 10% change in difference between CH_4 molecule polarizabilities in the ground and excited vibrational states changes shift coefficients more than two-fold.

For the considered transitions in methane, the truncation radius b_0 of the Anderson theory is significantly larger than the distance of the closest approach between CH_4 and SF_6 molecules in collisions. Therefore, our calculation does not take into account the close-range part of interaction potential and trajectory bending in colliding. It is evident however, that accounting for the close-range forces slightly increases the calculated value of the line half-width.

The CH_4 line half-widths induced by collisions with SF_6 were measured and calculated earlier.[22] The experimental value (0.093 cm^{-1}/atm) for the doublet line P7F of the ν_3 band and the calculated one (0.0857 cm^{-1}/atm) are in agreement with our result (0.068 cm^{-1}/atm). The agreement for mean values of shift coefficients is slightly worse (about 20%).

Acknowledgements

The authors are grateful to A.V. Nikitin for the data on quantum identification of 6046.96 cm^{-1} line of CH_4 and to V.M. Mikhailov for useful discussions.

References

1. T. Gabard, J. Quant. Spectrosc. and Radiat. Transfer **57**, No. 2, 177–196 (1997).
2. V.D. Malathy, D.C. Benner, M.A.H. Smith, and C.P. Rinsland, J. Mol. Spectrosc. **157**, No. 1, 95–111 (1993).
3. P. Varanasi, J. Quant. Spectrosc. and Radiat. Transfer **14**, No. 10, 995–1008 (1974).
4. G.D. Tejwani, P. Varanasi, and K. Fox, J. Quant. Spectrosc. and Radiat. Transfer **15**, No. 3, 243–254 (1975).
5. S.P. Neshyba, R. Lynch, R. Gamache, T. Gabard, and J.-P. Champion, J. Chem. Phys. **101**, No. 11, 9412–9421 (1994).
6. T. Gabard, J. Quant. Spectrosc. and Radiat. Transfer **59**, Nos. 3–5, 287–302 (1998).
7. A.S. Pine, J. Quant. Spectrosc. and Radiat. Transfer **57**, No. 2, 145–155 (1979).
8. A.S. Pine, J. Quant. Spectrosc. and Radiat. Transfer **57**, No. 2, 157–176 (1979).
9. A.S. Pine and T. Gabard, J. Quant. Spectrosc. and Radiat. Transfer **66**, No. 1, 69–92 (2000).
10. I.M. Grigoriev, N.N. Filippov, M.V. Tonkov, T. Gabard, and R. Le Doucen, J. Quant. Spectrosc. and Radiat. Transfer **69**, No. 2, 189–204 (2001).
11. I.M. Grigoriev, N.N. Filippov, M.V. Tonkov, T. Gabard, and R. Le Doucen, J. Quant. Spectrosc. and Radiat. Transfer **74**, No. 4, 431–443 (2002).
12. T. Gabard, I.M. Grigoriev, N.M. Grigorovich, and M.V. Tonkov, J. Mol. Spectrosc. **225**, No. 2, 123–131 (2004).
13. D. Pieroni, Nguyen-Van-Thanh, C. Brodbeck, J.-M. Hartmann, T. Gabard, J.-P. Champion, D. Bermejo, J.-L. Domenech, C. Claveau, and A. Valentin, J. Chem. Phys. **113**, No. 14, 5776–5783 (2000).
14. D. Pieroni, J.-M. Hartmann, F. Chaussard, X. Michaut, T. Gabard, R. Saint-Loup, H. Berger, and J.-P. Champion, J. Chem. Phys. **112**, No. 3, 1335–1343 (2000).
15. D. Pieroni, Nguyen-Van-Thanh, C. Brodbeck, J.-M. Hartmann, T. Gabard, J.-P. Champion, D. Bermejo, J.-L. Domenech, C. Claveau, A. Valentin, M.V. Tonkov, I.M. Grigoriev, and R. Le Doucen, J. Chem. Phys. **111**, No. 15, 6850–6863 (1999).
16. D. Pieroni, Nguyen-Van-Thanh, C. Brodbeck, C. Claveau, A. Valentin, J.-M. Hartmann, T. Gabard, J.-P. Champion, D. Bermejo, and J.-L. Domenech, J. Chem. Phys. **110**, No. 16, 7717–7732 (1999).
17. J.K.G. Watson, J. Mol. Spectrosc. **40**, Nos. 1–3, 536–544 (1971).
18. K. Fox, Phys. Rev. Lett. A **27**, No. 5, 233–236 (1971).
19. I. Ozier, Phys. Rew. Lett. **27**, No. 20, 1329–1332 (1971).
20. S.P. Gavva and V.M. Mikhailov, in: *High Resolution Spectroscopy of Small Molecules* (Nauka, Moscow, 1988), pp. 149–195.
21. H. Sasada, K. Suzmura, and Ch. Isehibashi, J. Chem. Phys. **105**, 9024–9034 (1996).
22. H.J. Gerritsen and M.E. Heller, Appl. Opt. Suppl. **2**, 73 (1965).
23. G.D. Tejwani and K. Fox, J. Quant. Spectrosc. and Radiat. Transfer **37**, No. 6, 541–546 (1987).
24. http://www.scitec.uk.com
25. http://www.nsu.ru/srd/lls/english/angstrom.htm
26. V. Zeninary, V.A. Kapitanov, Yu.N. Ponomarev, and D. Courtois, Infrared Phys. Technol. **40**, No. 1, 1–23 (1999).
27. V. Zeninary, B. Parvitte, D. Courtois, V.A. Kapitanov, and Yu.N. Ponomarev, Appl. Phys. B **72**, No. 7, 953–959 (2001).
28. V. Raynes, W.T. Lazzeretti, and P. Zanasi, Mol. Phys. **64**, No. 6, 1061–1071 (1988).
29. A.A. Ratsig and B.M. Smirnov, *Handbook on Atomic and Molecular Physics* (Atomizdat, Moscow, 1980), 238 pp.